Large Eddy simulation of a spray jet flame using filtered tabulated chemistry

Adrien Chatelier, Benoit Fiorina, Vincent Moureau, Nicolas Bertier

10.2514/6.2019-2144

Large Eddy simulation of a spray jet flame using filtered tabulated chemistry

Adrien Chatelier * and Benoît Fiorina †
Laboratoire EM2C, CNRS, CentraleSupélec, 91192 Gif-sur-Yvette cedex, France

Vincent Moureau ‡
Normandie Univ, INSA Rouen, UNIROUEN, CNRS, CORIA, 76000 Rouen, France

Nicolas Bertier §
ONERA - The French Aerospace Lab - Centre de Châtillon, BP 72 - 92322 CHATILLON CEDEX, France

Large Eddy Simulation of a liquid n-heptane/air laboratory jet burner using the Filtered TAbulated Chemistry model for LES (F-TACLES) is presented. This work aims to address the ability of the F-TACLES model to retrieve the correct turbulent spray flame structure. LES results are compared against experimental measurements in terms of heat release, spray properties and flow characteristics. Numerical simulations recover both the flame lift-off and the double flame structure found in the experiments. For non-reacting and reacting conditions, the gas phase velocity as well as the mean droplet diameter are well retrieved, whereas differences are observed for the droplet temperature. An analysis is conducted which tends to attribute the cause of observed discrepancies to the evaporation model assumptions.

I. Introduction

Aeronautical engines are operated with liquid fuel directly injected in the combustor. Two-phase combustion is extremely difficult to understand as it requires a simultaneous access to a large number of highly-correlated thermo-physical properties [1]. The Large Eddy Simulation (LES) approach represents nowadays the best compromise between cost and accuracy to simulate complex reactive flows. Despite recent impressive progress, many efforts are still performed by the combustion modeling community to develop and validate LES for turbulent spray flame computational strategies [2–6]. Model comparison against accurate experimental data is crucial to properly assess the ability of numerical strategies to recover the turbulent spray flame properties. It includes the flow velocity, the droplets characteristics and the flame structure.

Flame stabilization and pollutant formation requires a fine description of the combustion kinetics [7]. Tabulated chemistry methodologies have been developed during the last decades to account for detailed chemistry effects at a

*Research Engineer, MBDA, adrien.chatelier@centralesupelec.fr
†Professor, CentraleSupélec, benoit.fiorina@centralesupelec.fr
‡CNRS research fellow, CORIA, vincent.moureau@coria.fr
§Research Engineer, ONERA, nicolas.bertier@onera.fr

reduced CPU cost [8, 9]. Among them, the Filtered Tabulated Chemistry for LES (F-TACLES), has been especially developed to incorporate complex chemistry effects in an LES formalism [10]. It consists in tabulating the chemical ingredients needed by the LES in a filtered lookup table. F-TACLES has been applied to complex gaseous turbulent flames such as stratified [11] and non-adiabatic [12, 13] configurations. The suitability of F-TACLES to turbulent spray flames simulations has however never been addressed, which is the main objective of this article.

The present work presents the first application of the filtered tabulated chemistry model F-TACLES in a turbulent spray combustion configuration. The retained configuration is a new well-instrumented experimental turbulent spray flame that has been designed and operated at CORIA laboratory [14]. Simulations are conducted on two different grids: a coarse one, representative of meshing constrains encountered in industrial applications, and a fine one for which the size of the cells within the reaction zones has been chosen so that both flame thickness and subgrid flame wrinkling are fully resolved. The fine grid simulation will challenge the ability of the chemistry tabulation to retrieve the spray flame structure [15], whereas the coarse LES will also test the suitability of F-TACLES to capture unresolved interactions between the spray flame and turbulence. Experimental and numerical data are compared and analyzed in terms of gas velocity, spray diameter distribution and velocity, flame structure and spray temperature.

II. Turbulent spray combustion modeling

The turbulent combustion model chosen in this study is the F-TACLES formalism, developed first for premixed combustion [10] and then extended to stratified flames [11]. The impact of differential diffusion effects on the flame consumption has been added by Mercier *et al.* [12]. In addition to the filtered flow governing equation, the F-TACLES model requires the solving of two balance equations for the mixture fraction $\widetilde{z}$ and the progress variable $\widetilde{Y_c}$, respectively:

$$\frac{\partial \bar{\rho}\widetilde{z}}{\partial t} + \frac{\partial}{\partial x_i}(\bar{\rho}\widetilde{u_i}\widetilde{z}) = \frac{\partial}{\partial x_i}\left(\left(\overline{\rho D_{th}} + \frac{\mu_t}{Sc_t}\right)\frac{\partial \widetilde{z}}{\partial x_i}\right) + \widetilde{\dot{\omega}}_{evap} \tag{1}$$

$$\frac{\partial \overline{\rho}\widetilde{Y_c}}{\partial t} + \frac{\partial}{\partial x_i}(\overline{\rho}\widetilde{u_i}\widetilde{Y_c}) = \frac{\partial}{\partial x_i}\left(\Xi_\Delta \alpha_{Y_c}[\widetilde{Y_c}, \widetilde{z}]\rho_0 D_0 \frac{\partial \widetilde{Y_c}}{\partial x_i}\right) \tag{2}$$

$$+ \Xi_\Delta \Omega_{Y_c}[\widetilde{Y_c}, \widetilde{z}] + \Xi_\Delta \overline{\rho}\widetilde{\dot{\omega}}_{Y_c}[\widetilde{Y_c}, \widetilde{z}] \tag{3}$$

where ρ is the density, D_{th} the thermal diffusivity, μ_t the turbulent viscosity, Sc_t the turbulent Schmidt number, $\widetilde{\dot{\omega}}_{evap}$ the source term of mixture fraction due to the evaporation of the spray, Ξ_Δ the subgrid scale flame wrinkling , α_{Y_c} the progress variable diffusion factor, ρ_0 the density in fresh gases, D_0 the diffusion coefficient in fresh gases, Ω_{Y_c} the progress variable unresolved convective fluxes due to thermal expansion and $\widetilde{\dot{\omega}}_{Y_c}$ the progress variable reaction rate. The terms α_{Y_c}, Ω_{Y_c} and $\widetilde{\dot{\omega}}_{Y_c}$ are tabulated by filtering 1-D adiabatic premixed flame elements computed including

detailed chemistry and complex transport and stored in a look-up table as a function of the mixture fraction $\widetilde{z}$, the progress variable $\widetilde{Y_c}$ and the filter size Δ.

The spray is described with a Lagrangian point-force approach, which is two-way coupled to the gaseous phase. The following transport equations are solved for each droplet:

$$\frac{d\mathbf{x}_p}{dt} = \mathbf{u}_p \tag{4}$$

$$m_p \frac{d\mathbf{u}_p}{dt} = m_p(\mathbf{u}_p - \mathbf{u}) \frac{3C_D Re_p \rho \nu}{4\rho_p d_p^2} \text{ with } Re_p = \frac{d_p|\mathbf{u}_p - \mathbf{u}|}{\nu} \tag{5}$$

where $\mathbf{x}_p$ is the particle position, $\mathbf{u}_p$ the particle velocity, $\mathbf{u}$ the gas velocity, m_p the particle mass, C_D the drag coefficient, ν the kinematic viscosity, ρ_p the particle density and Re_p the particle Reynolds number.

The evaporation of the spray is modelled with the classical approach derived by Spalding [16]. The droplet mass transfer equation reads:

$$\dot{m}_p = -\pi d_p \rho \mathcal{D} Sh \log(1 + B_M) \tag{6}$$

where d_p is the particle diameter, $\mathcal{D}$ is the diffusion coefficient, Sh the Sherwood number and B_M the Spalding mass number. The term $\widetilde{\dot{\omega}}_{evap}$ in the mixture fraction equation is obtained by adding the mass transfer contribution of all the droplets around each node of the mesh:

$$\widetilde{\dot{\omega}}_{evap} = -\frac{1}{V_{node}} \sum_{droplet \in node} \dot{m}_p \tag{7}$$

where V_{node} is the volume around the node. The other droplet parameters are derived by integrating either the droplet mass or energy equations. Droplet temperature T_p and diameter d_p are obtained by solving the following set of equations:

$$\frac{\mathrm{d}T_p}{\mathrm{d}t} = -\frac{1}{\tau_p}\left(T_p - \left(T_\infty - \frac{L_v B_T}{C_{p,1/3}}\right)\right) \tag{8}$$

$$\frac{\mathrm{d}d_p^2}{\mathrm{d}t} = -\frac{2Sh\mu_{1/3}\log(1 + B_M)}{d_p \rho_p Sc} \tag{9}$$

$$\tau_p = \frac{\rho_p d_p^2}{6} \frac{Sc}{Sh \cdot \mu_{1/3}} \frac{C_{p,k}}{C_{p,1/3}} \frac{B_T}{\log(1 + B_M)} \tag{10}$$

where τ_p is the thermal characteristic time of the Spalding model, T_∞ the gas temperature in the far field, L_v the

latent heat of vaporarization of the fuel, B_T the Spalding thermal number, $C_{p,1/3}$ the heat capacity at a classical reference state assuming a one third/two third equilibrium between the far field and the droplet surface, $\mu_{1/3}$ the dynamic viscosity at the same reference state and S_c the Schmidt number.

III. Experimental configuration

The experimental configuration is an n-heptane spray/air jet burner experimented at CORIA by Verdier et al. [14]. It is operated at atmospheric pressure and 298 K. The air injection is performed from a plenum to a non-swirling injector in order to generate the co-flow where the liquid fuel is atomized. The air mass flow rate of is 6 g.s^{-1}. The injection of liquid n-heptane comes from a simplex injector that generates a hollow cone with a mass flow rate of 0.28 g.s^{-1}. A general view of the configuration geometry is shown in Fig. 1.

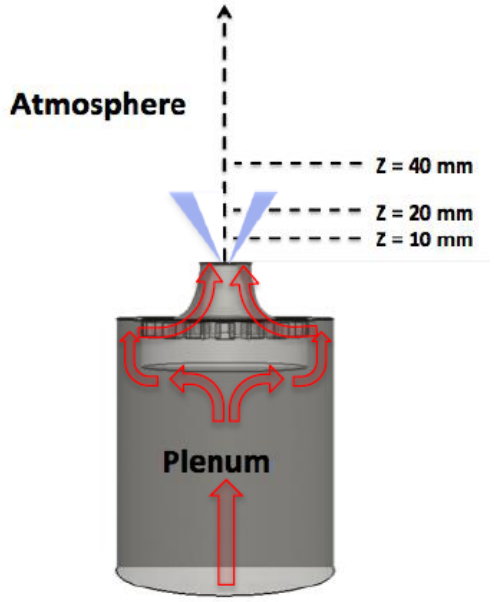

Fig. 1 Experimental setup. Air path in red, spray injection in blue. From [4].

Several experimental measurements have been performed. The Phase Doppler Anemometry (PDA) gives access to the gas and spray velocity and the spray diameter distribution. The flame structure is determined thanks to OH Planar Laser Induced Fluorescence (PLIF). Finally, the Global Rainbow Technique (GRT) [17] provides the spray temperature, which is rarely available in experimental diagnostics. Further details about these measurements can be found in [14].

The flame structure shown by the OH-PLIF measurement exhibits a double branch. The inner flame front corresponds to a premixed flame where the small droplets are vaporized rapidly and the high levels of turbulence favor the air/fuel mixing, forming a highly wrinkled flame front. The outer flame front is closer to a diffusion flame, where air located outside reacts with rich hot gases still containing a large amount of unburnt gaseous n-heptane. OH-PLIF also shows

Table 1 Studied cases.

Case	A	B
Elements (million)	53	17
F-TACLES Filter size Δ (mm)	0.0	3.5
Subgrid flame wrinkling Ξ_Δ	1.0	[24]

that the flame is lifted from the injection plane.

IV. Numerical Setup

This experiment has been previously studied numerically by Shum-Kivan et al. [4] by using a global two-step chemistry [18] combined with the TFLES approach [19, 20]. The flow velocity, as well as the droplet size distribution and velocity have been well predicted. However, an underestimation of the flame lift-off has been observed, which is probably due to the limitation of the reduced two-step chemistry model. Other approaches were tested on this configuration, for example with the stochastic fields method [21].

The computational domain defined in [4] is also used in the present study. Two cases (A and B) are considered in this study. Case A features an unstructured mesh composed of 53 million elements and 10.5 million nodes, identical to [4]. Case B is performed on a coarser mesh of 17 million elements and 3.5 million nodes. Case A is sufficiently resolved so that artificial broadening of the flame front is not required. Indeed, the mesh size in the reaction zone is less than 0.1 mm, whereas the minimum possible flame thickness, given by a laminar stoichiometric premixed freely propagating flames, is about 0.5 mm. With 5 nodes accross the flame front, the resolution of the chemical layer is therefore sufficient to ensure the proper propagation of the flame without introducing numerical artifact [10]. The flame front resolution in Case B is more representative of LES conditions encountered in industrial configurations. The mesh size in the reaction zone, around 0.5 mm, is not sufficient to resolve the flame front.

The chemical table is built from a library of laminar freely propagating n-heptane/air premixed flamelet computed with the REGATH code [22] and by using the POLIMI 106 detailed mechanism made of 106 species and 1738 reactions [23]. For case A simulation, as the flame is fully resolved on the LES mesh, this look-up table is directly used to close Eq. 3 without being filtered ($\Delta = 0$). Consequently, by assuming flamelet regime, the flame wrinkling is also fully resolved on the LES grid and $\Xi_\Delta = 1$. At the opposite, the flamelets library is filtered in Case B by using a filter width $\Delta = 3.5$ mm so that the resolved filtered flame thickness is sufficient to capture the flame consumption speed on the coarse mesh. Subgrid scale flame wrinkling is modelled as in Charlette *et al.* [24]. Combustion model properties used for case A and B are summarized in Table 1.

The YALES2 flow solver is used [25]. The time integration relies on a low-Mach number projection method for variable density flows. The temporal integration and spatial discretization are of fourth order. The subgrid scale

Reynolds stresses are closed with the SIGMA model [26].

The injected spray is polydispersed in size, following a two-parameter Rosin-Rammler distribution [27] with a Sauter Mean Diameter (SMD) d_{32} of 31 microns and a spread parameter q of 2.3. The form of the injected spray is obtained with the Liquid Injection for Swirl Atomizers (LISA) formalism [28] to obtain the desired swirled hollow cone spray. Parameters of droplet distribution in size are empirically adjusted to fit measurements at 10 mm above the burner exit as shown in Figure 2.

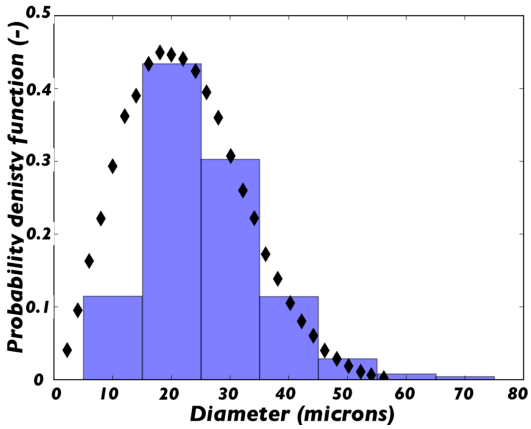

Fig. 2 Particle size distribution. Experiments: blue bars, Rosin-Rammler distribution: black diamonds.

V. Results and analysis

The two cases A and B are computed in both non-reactive and reactive configurations.

For the cold flow configuration, LES axial and radial gas velocity components are compared against the measurements at 10, 20 and 40 mm high above the burner exit in Fig. 3. Both cases A and B solutions match well the experimental data, meaning that the flow statistics are well captured, even on the coarse grid. Reactive results are plotted in Fig. 4. The comparison of gas velocity predicted by LES against the experimental data shows also a good reproduction of the flow topology.

Figure 5 compares at 10, 20 and 40 mm high above the burner exit, the mean spray diameter as a function of the radial coordinates for the cold and reacting cases, respectively. The LES results show a correct evolution of the radial stratification in droplet diameter for both cases A and B. The small droplets follow the streamlines because of their small Stokes number and are therefore located at the center of the flow. The larger droplets, characterized by a higher Stokes number, follow a ballistic trajectory and are located on the outer rim of the spray, as a result of the hollow cone injection. The profiles are similar in both reacting and non-reacting cases between 0 and 20 mm, as flame is located further downstream. The smaller diameters encountered at 40 mm in the reacting case are the result of the stronger evaporation process due to the presence of the flame. This phenomenon is well captured by the F-TACLES model, even

in case B where subgrid scale contributions are significant.

Droplets velocity is reported in Fig. 6 for the cold and reacting cases, respectively. The experimental measurements are colored by the diameter of the spray at the considered radial position. Green squares correspond to particle diameters lower than 15 microns, blue squares to diameters between 15 and 35 microns and red squares to diameters larger than 35 microns. The agreement is good for small to medium droplets (below 35 microns), but both LES cases predicts a higher velocity than the experiments for the large droplets.

Figure 7 shows an instantaneous normalized OH mass fraction field for each simulated case and an instantaneous snapshot of OH-PLIF measurements to compare qualitatively the instantaneous flame structure. The flame structure is challenging to compute because the flame structure as well as the stabilization process are very sensitive to finite-rate chemistry effects. The inner flame front, characterized by a high resolved wrinkling, is correctly reproduced. The outer diffusion flame observed in the experiments, featuring a large and unwrinkled reaction zone, is also present. The lift-off of the flame, estimated in the simulations as the lowest height where heat release is detected is well captured in the simulations, which is a critical aspect of this flame. The experimental value is 25±3 mm while case A recovers a lift-off of 22±1 mm and case B a lift-off of 24±1 mm. Comparison between case A and B shows that the F-TACLES approach is able to model fairly well unresolved flame turbulence interaction on mesh representative of practical industrial conditions.

Previously published computations with a crude global-step mechanism [4] underpredict the flame lift-off h_{lo} by approximately 20%. Figure 7 shows that the flame position and structure is here well retrieved in both LES by qualitative comparison with OH-PLIF snapshot. Moreover, computations conducted with a reduced analytical scheme involving 24 transported species, 32 quasi-steady state species and 217 reactions did not succeed to retrieve the flame lift-off, with a CPU cost 10 times higher [29]. With the F-TACLES tabulated chemistry method, the flame lift-off height is recovered for both meshes and for a CPU cost even lower than the global mechanism. The good performances of F-TACLES are due to its ability to retrieve the flame propagation speed in turbulent stratified mixture [11], even on coarse grid where the flame front is not resolved.

Table 2 compares against experiments the flame lift-off heigh predicted by global, analytical and tabulated chemistry on the investigated spray flame configuration. The CPU cost required to obtained reactive flow statistics, normalized by the global scheme computation, is also indicated.

Table 2 Comparison between chemistry modeling strategies.

	Experiment	Two-steps scheme [3]	Analytical scheme [3]	F-TACLES	F-TACLES
Grid	-	fine	fine	fine	coarse
Lift-off (mm)	25±3	20±1	20±1	24±1	22±1
Estimated relative CPU cost	-	1	10	0.5	0.1

Finally, the droplet temperature predicted by the LES is compared with the Global Rainbow Technique (GRT) measurements. Figure 8 presents axial profiles of temperature for the cold configuration. The experimental data highlight two zones. For $r > 5$ mm, the droplets reach quickly the wet bulb temperature, from the first measured radial profiles, i.e. 20 mm above the burner exit, whereas the liquid spray remains at the injection temperature around the centerline. This trend is not captured by the simulation, which predicts the wet bulb temperature for all droplet positions. This difference between simulations and experiments could be explained by limitations of the evaporation model [30]. Another possible explanation would be the weakness of the injection model, which, by injecting all droplets from the same point, does not reproduce the spatial distribution of droplets induced by the liquid sheet break-up. Despite a correct prediction of the overall particle size, a local misprediction of the droplet distribution would also impact the mean liquid temperature.

Droplet temperature of the reactive configuration are shown in Fig.9. In the burnt gases region, located at $r > 10$ mm and $z > 20$ mm, the droplet temperature rises quickly due to the high gas temperature in this zone. This phenomenon observed in the experiments is fairly tackled by the simulations. However, the droplet temperature measured downstream, between the inner and the outer branch of the flame, reaches a thermal equilibrium around 331 K whereas the numerical simulation predicts 367 K, which is close to the boiling temperature of n-heptane. As discussed in [31], this discrepancy may be attributed to the Spalding evaporation model, where the limiting value is the boiling temperature.

VI. Conclusion

The first simulation with the F-TACLES formalism in a spray combustion configuration has been performed. The results show good agreement on the spray diameter and velocity, gas velocity, flame structure and lift-off with respect to experimental data. The complex flame structure, which presents a inner premixed flame front and an outer diffusion branch, is well reproduced by the simulation, even on the coarse grid representative of meshing conditions encountered in industrial applications. Case A simulations showed that tabulated chemistry based on premixed flamelets is adequate to capture the spray flame chemistry. The good prediction obtained on the coarse grid also demonstrates the ability of F-TACLES to model the unresolved interactions between the spray flame and turbulence. As the supplementary CPU cost induced by the combustion model is very low, this method is of interest for the gas turbine engineering community. However, another issue remains to be addressed. Significant discrepancies are indeed found for the droplet temperature. The influence of the droplet evaporation model and of the liquid sheet atomization on the spray temperature should be investigated in the future.

Acknowledgments

This work was performed using HPC resources from GENCI-IDRIS (Grants 2016-x20162b0164 and 2017-x2017b0164). We acknowledge Antoine Verdier and Bruno Renou from CORIA laboratory for sharing the experimental

data and for the fruitful discussions. We also are grateful of Francis Shum-Kivan, Eléonore Riber and Bénédicte Cuénot for sharing the geometry and mesh of the computational domain and for the helpful discussions.

References

[1] Jenny, P., Roekaerts, D., and Beishuizen, N., "Modeling of turbulent dilute spray combustion," *Progress in Energy and Combustion Science*, Vol. 38, No. 6, 2012, pp. 846–887.

[2] Jones, W. P., Marquis, A. J., and Noh, D., "An investigation of a turbulent spray flame using Large Eddy Simulation with a stochastic breakup model," *Combustion and Flame*, Vol. 186, No. Supplement C, 2017, pp. 277 – 298. doi:https://doi.org/10.1016/j.combustflame.2017.08.019, URL http://www.sciencedirect.com/science/article/pii/S0010218017303164.

[3] Jones, W., Marquis, A., and Vogiatzaki, K., "Large-eddy simulation of spray combustion in a gas turbine combustor," *Combustion and Flame*, Vol. 161, No. 1, 2014, pp. 222 – 239. doi:https://doi.org/10.1016/j.combustflame.2013.07.016, URL http://www.sciencedirect.com/science/article/pii/S0010218013002861.

[4] Shum-Kivan, F., Santiago, J. M., Verdier, A., Riber, E., Renou, B., Cabot, G., and Cuenot, B., "Experimental and numerical analysis of a turbulent spray flame structure," *Proceedings of the Combustion Institute*, 2016.

[5] Franzelli, B., Vié, A., Boileau, M., Fiorina, B., and Darabiha, N., "Large Eddy Simulation of Swirled Spray Flame Using Detailed and Tabulated Chemical Descriptions," *Flow, Turbulence and Combustion*, 2016, pp. 1–29.

[6] Heye, C., Raman, V., and Masri, A. R., "Influence of spray/combustion interactions on auto-ignition of methanol spray flames," *Proceedings of the Combustion Institute*, Vol. 35, No. 2, 2015, pp. 1639 – 1648. doi:https://doi.org/10.1016/j.proci.2014.06.087, URL http://www.sciencedirect.com/science/article/pii/S1540748914002454.

[7] Pope, S. B., "Small scales , many species and the manifold challenges of turbulent combustion," *Proceedings of the Combustion Institute*, Vol. 34, No. 1, 2013, pp. 1–31. doi:10.1016/j.proci.2012.09.009, URL http://dx.doi.org/10.1016/j.proci.2012.09.009.

[8] Fiorina, B., Veynante, D., and Candel, S., "Modeling combustion chemistry in large eddy simulation of turbulent flames," *Flow, Turbulence and Combustion*, Vol. 94, No. 1, 2015, pp. 3–42. doi:10.1007/s10494-014-9579-8.

[9] Oijen, J. A. V., Donini, A., Bastiaans, R. J. M., Boonkkamp, J. H. M. T., and Goey, L. P. H. D., "State-of-the-art in premixed combustion modeling using flamelet generated manifolds," *Progress in Energy and Combustion Science*, Vol. 57, 2016, pp. 30–74. doi:10.1016/j.pecs.2016.07.001, URL http://dx.doi.org/10.1016/j.pecs.2016.07.001.

[10] Fiorina, B., Vicquelin, R., Auzillon, P., Darabiha, N., Gicquel, O., and Veynante, D., "A filtered tabulated chemistry model for LES of premixed combustion," *Combustion and Flame*, Vol. 157, No. 3, 2010, pp. 465 – 475.

[11] Auzillon, P., Gicquel, O., Darabiha, N., Veynante, D., and Fiorina, B., "A Filtered Tabulated Chemistry model for LES of stratified flames," *Combustion and flame*, Vol. 159, No. 8, 2012, pp. 2704–2717.

[12] Mercier, R., Auzillon, P., Moureau, V., Darabiha, N., Gicquel, O., Veynante, D., and Fiorina, B., "LES Modeling of the Impact of Heat Losses and Differential Diffusion on Turbulent Stratified Flame Propagation: Application to the TU Darmstadt Stratified Flame," *Flow, Turbulence and Combustion*, Vol. 93, No. 2, 2014, pp. 349–381.

[13] Mercier, R., Guiberti, T., Chatelier, A., Durox, D., Gicquel, O., Darabiha, N., Schuller, T., and Fiorina, B., "Experimental and numerical investigation of the influence of thermal boundary conditions on premixed swirling flame stabilization," *Combustion and Flame*, Vol. 171, 2016, pp. 42–58.

[14] Verdier, A., Santiago, J. M., Vandel, A., Saengkaew, S., Cabot, G., Grehan, G., and Renou, B., "Experimental study of local flame structures and fuel droplet properties of a spray jet flame," *Proceedings of the Combustion Institute*, 2016.

[15] Franzelli, B., Fiorina, B., and Darabiha, N., "A tabulated chemistry method for spray combustion," *Proceedings of the Combustion Institute*, Vol. 34, No. 1, 2013, pp. 1659–1666.

[16] Spalding, D. B., "The combustion of liquid fuels," *Symposium (international) on combustion*, Vol. 4, Elsevier, 1953, pp. 847–864.

[17] Saengkaew, S., Bodoc, V., Lavergne, G., and Grehan, G., "Application of global rainbow technique in sprays with a dependence of the refractive index on droplet size," *Optics Communications*, Vol. 286, 2013, pp. 295–303.

[18] Paulhiac, D., "Modélisation de la combustion d'un spray dans un brûleur aéronautique," Ph.D. thesis, 2015.

[19] Legier, J.-P., Poinsot, T., and Veynante, D., "Dynamically thickened flame LES model for premixed and non-premixed turbulent combustion," *Proc. of the summer program*, Citeseer, 2000, pp. 157–168.

[20] Colin, O., Ducros, F., Veynante, D., and Poinsot, T., "A thickened flame model for large eddy simulations of turbulent premixed combustion," *Physics of Fluids*, Vol. 12, No. 7, 2000, pp. 1843–1863.

[21] Gallot Lavallee, S., Noh, D., Jones, W., Navarro-Martinez, S., Verdier, A., Marrero Santiago, J., Cabot, G., and Renou, B., "Experimental and numerical study of turbulent flame structures of a spray jet flame," *European Combustion Meeting*, Combustion Institute, 2017.

[22] Darabiha, N., "Transient behaviour of laminar counterflow hydrogen-air diffusion flames with complex chemistry," *Combustion science and technology*, Vol. 86, No. 1-6, 1992, pp. 163–181.

[23] Ranzi, E., Frassoldati, A., Stagni, A., Pelucchi, M., Cuoci, A., and Faravelli, T., "Reduced kinetic schemes of complex reaction systems: fossil and biomass-derived transportation fuels," *International Journal of Chemical Kinetics*, Vol. 46, No. 9, 2014, pp. 512–542.

[24] Charlette, F., Meneveau, C., and Veynante, D., "A power-law flame wrinkling model for LES of premixed turbulent combustion Part I: non-dynamic formulation and initial tests," *Combustion and Flame*, Vol. 131, No. 1, 2002, pp. 159–180.

[25] Moureau, V., Domingo, P., and Vervisch, L., "Design of a massively parallel CFD code for complex geometries," *Comptes Rendus Mécanique*, Vol. 339, No. 2, 2011, pp. 141–148.

[26] Nicoud, F., Toda, H. B., Cabrit, O., Bose, S., and Lee, J., "Using singular values to build a subgrid-scale model for large eddy simulations," *Physics of Fluids (1994-present)*, Vol. 23, No. 8, 2011, p. 085106.

[27] González-Tello, P., Camacho, F., Vicaria, J., and González, P., "A modified Nukiyama–Tanasawa distribution function and a Rosin–Rammler model for the particle-size-distribution analysis," *Powder Technology*, Vol. 186, No. 3, 2008, pp. 278–281.

[28] Guedot, L., "Développement de méthodes numériques pour la caractérisation des grandes structures tourbillonnaires dans les brûleurs aéronautiques: application aux systèmes d'injection multi-points," Ph.D. thesis, Rouen, INSA, 2015.

[29] Shum-Kivan, F., "Simulation des Grandes Echelles de flammes de spray et modélisation de la combustion non-prémélangée," Ph.D. thesis, Institut National Polytechnique de Toulouse (INP Toulouse), 2017.

[30] Shashank, Knudsen, E., and Pitsch, H., "Spray evaporation model sensitivities," *Annual Research Briefs, Centre for Turbulence Research*, , No. 1998, 2011, pp. 213–224.

[31] Miller, R., Harstad, K., and Bellan, J., "Evaluation of equilibrium and non-equilibrium evaporation models for many-droplet gas-liquid flow simulations," *International Journal of Multiphase Flow*, Vol. 24, No. 6, 1998, pp. 1025–1055.

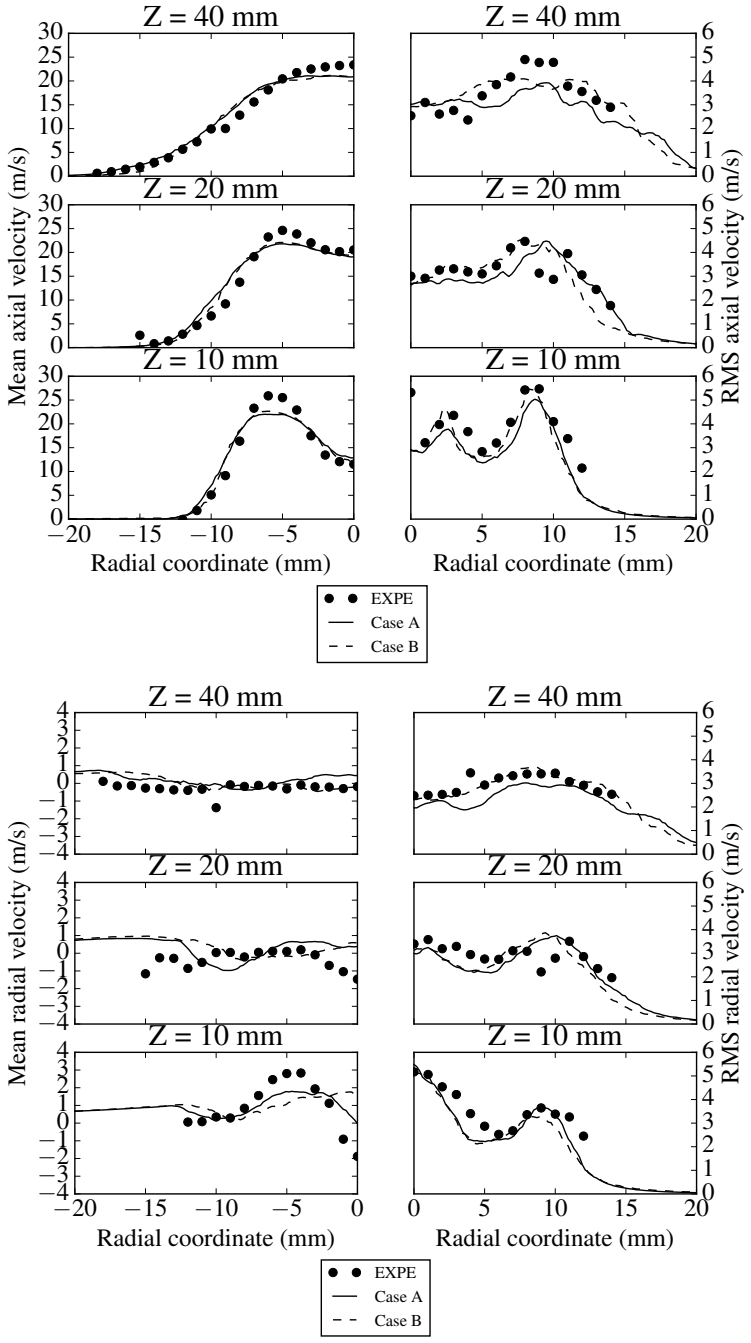

Fig. 3 Cold case mean and RMS gas axial (top) and radial (bottom) velocity. Symbols: experiments, solid line: Case A, dashed line: Case B.

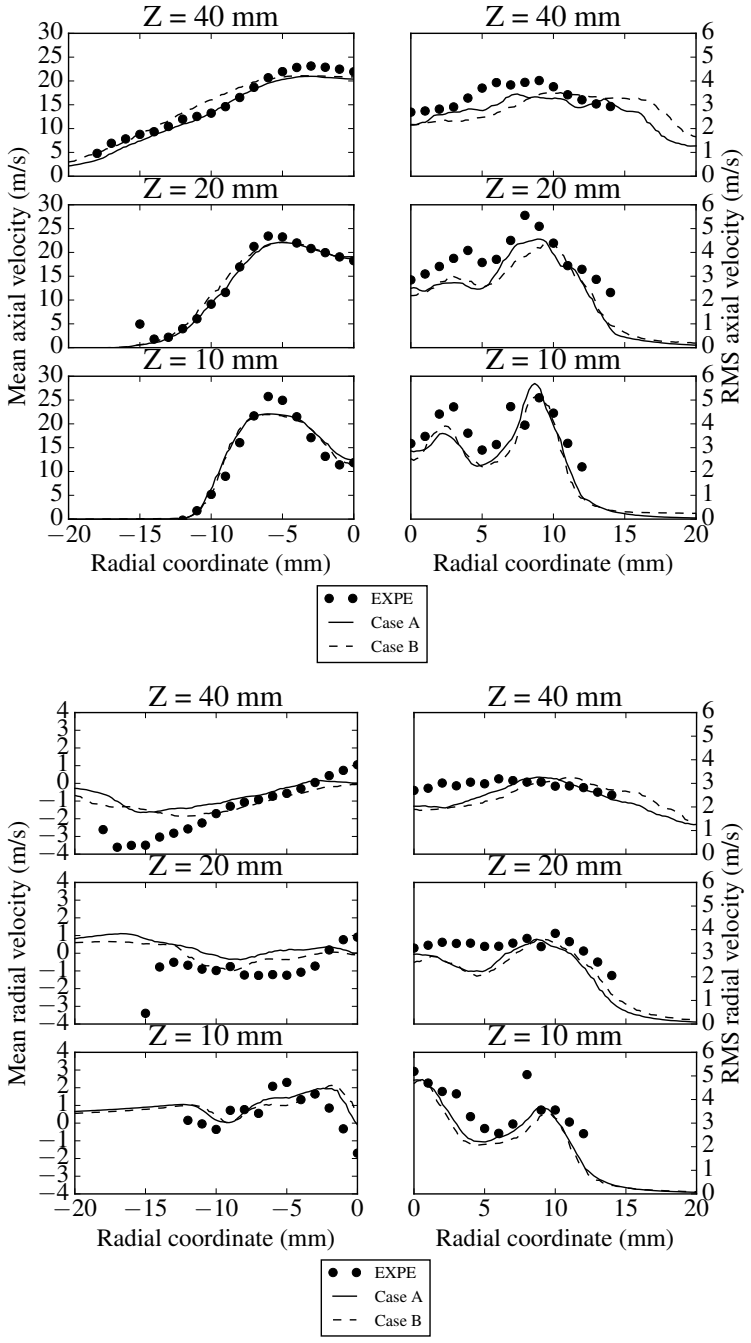

Fig. 4 Reacting case mean and RMS gas axial (top) and radial (bottom) velocity. Symbols: experiments, solid line: Case A, dashed line: Case B.

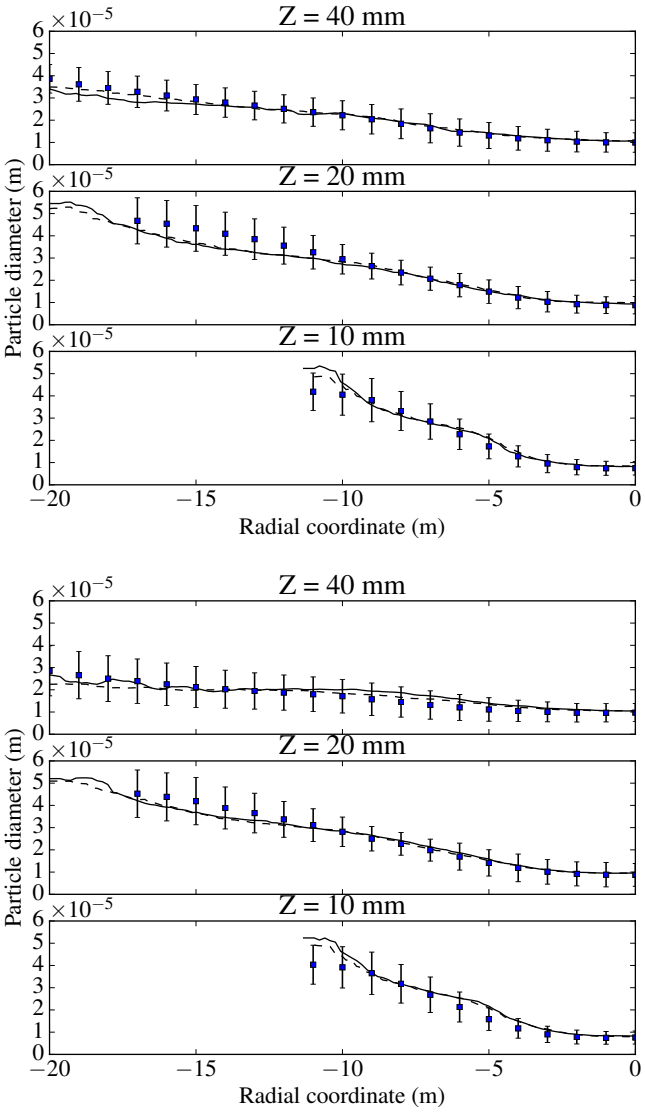

Fig. 5 Cold case (top) and reacting case (bottom) mean spray diameter. Symbols: experiments, solid line: Case A, dashed line: Case B.

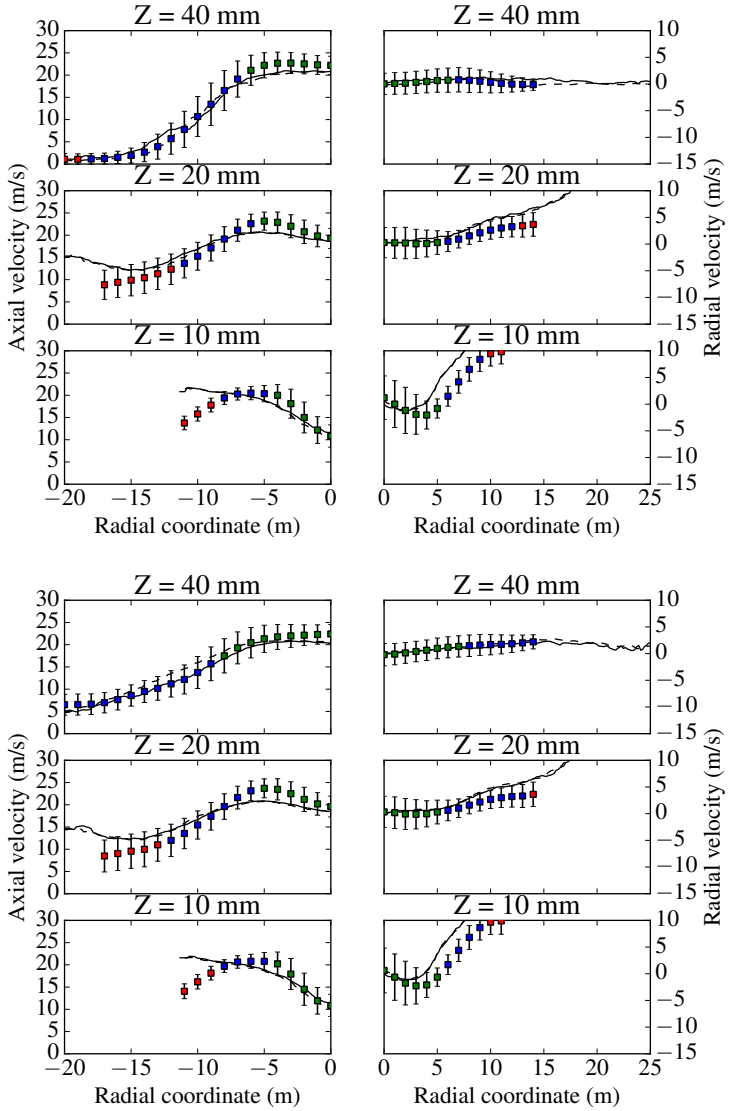

Fig. 6 Cold case (top) and reacting case (bottom) mean axial (left column) and radial (right column) spray velocity. Symbols: experiments (green: $d_p < 15$ mm, blue: $15 < d_p < 35$ mm, red: $35 < d_p$ mm), solid line: Case A, dashed line: Case B.

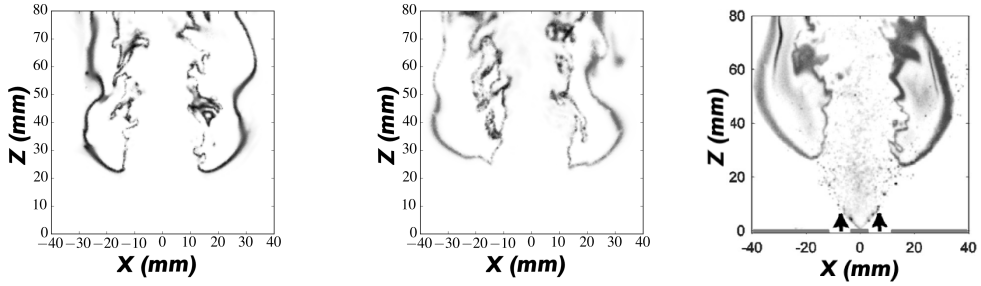

Fig. 7 Instantaneous normalized OH mass fraction (Case A: left, case B: middle). Experiments (right): instantaneous OH-PLIF shot, from [14].

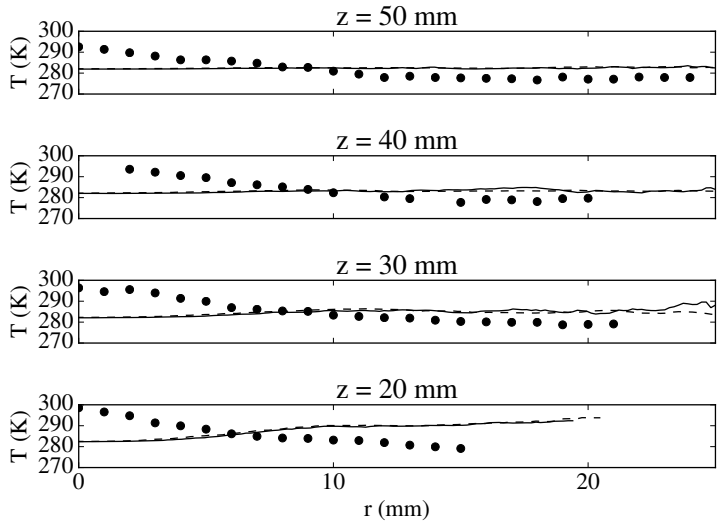

Fig. 8 Cold case radial profiles of mean spray temperature. Circles: experiments, solid line: Case A, dashed line: Case B.

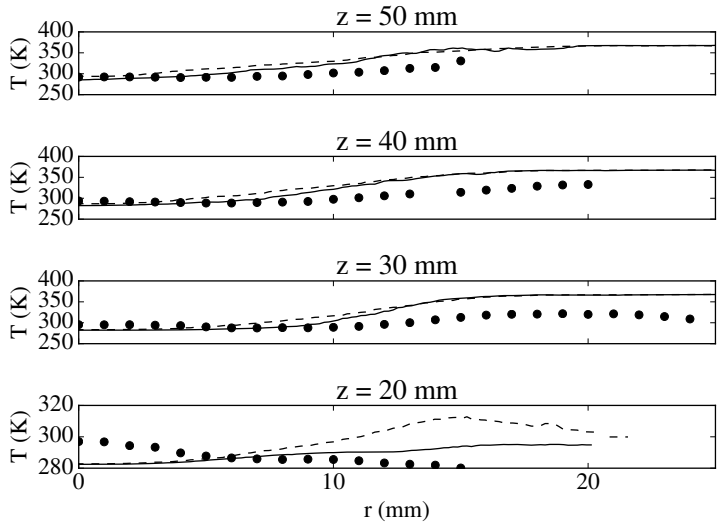

Fig. 9 Reacting case radial profiles of mean spray temperature. Symbols: experiments, solid line: Case A, dashed line: Case B.